P3HT as a Hole Transport Layer for Colloidal Quantum Dot Solar Cells

Darren C. J. Neo[1‡], Nanlin Zhang[1], Yujiro Tazawa[1], Haibo Jiang[1,2], Gareth M. Hughes[1], Chris R. M. Grovenor[1], Hazel E. Assender[1‡], Andrew A. R. Watt[1]‡*

[1] Materials Department, University of Oxford, 16 Parks Road

Oxford OX1 3PH, Oxford, United Kingdom.

[2] Centre for Microscopy, Characterisation and Analysis, The University of Western Australia, 35 Stirling Highway, Crawley 6009, Western Australia, Australia

KEYWORDS: Colloidal quantum dots, lead sulfide, hole transport layer, P3HT, solar cell

ABSTRACT: Lead sulfide colloidal quantum dot (CQD) solar cells demonstrate extremely high short-circuit currents (J_{sc}) and are making decent progress in power conversion efficiencies. However, the low fill factors (*FF*) and open-circuit voltages have to be addressed with urgency to prevent the stalling of efficiency improvements. This paper highlights the importance of improving hole extraction, which received much less attention as compared to the electron accepting component of the device architecture (eg. TiO_2 or ZnO). Here, we show the use of semiconducting polymer Poly(3-hexylthiophene-2,5-diyl) (P3HT) to create efficient CQD devices by improving hole transport, removing interfacial barriers and minimizing shunt

pathways, thus resulting in an overall improvement in device performance stemming from better J_{sc} and *FF*.

INTRODUCTION

Recently, solution processed CQD solar cells have seen certified power conversion efficiencies rise to 10.6 %[1] and an extended device stability in air[2,3]. These advances have been largely driven by improved surface chemistry[4], fabrication process engineering[5] and light trapping strategies[6]. However, at voltages around the maximum power point, charge transport is dominated by diffusive processes due to a reduction in the depletion width at the charge separating-junction, which results in poor fill factors[4]. At the same time, unbalanced charge extraction[7], shunt resistance losses arising from film inhomogeneities[5], and contact resistance/ Fermi level-pinning between the CQD film and metal electrode[8] also leads to low fill factors.

For further efficiency enhancement, we propose that CQD devices need to shift away from relying principally on drift for charge transport[7]and instead, we need to pay more attention to improving diffusive transport**.** Recent studies have shown that by using different ligands as the CQD film is built up layer-by-layer, a localized band bending at the rear junction is created, thus improving charge collection based on diffusive transport by imparting charge selectivity. These improvements have enhanced overall device performance and have raised the fill factor (*FF*) of up to 0.6[2]. The rear junction band bending is also recently demonstrated in a set of PbS and PbSe devices, with reports of efficient devices of up to 500 nm active layer thickness[9]. Another approach commonly used is to employ a hole transport material to balance charge extraction[10–12], which could simultaneously play a role as a smoothing interfacial layer between the active material and the top electrode[13]. In this paper, we examine the application of P3HT in a CQD

solar cell device with the structure as shown in fig. 1a. P3HT is a well-known *p*-type organic semiconductor with a relatively high hole mobility and the literature suggests suitable HOMO and LUMO levels with respect to 1.3 eV PbS CQD – to perform the role of promoting hole extraction and blocking electron injection into the rear electrode, as shown in fig. 1b. This therefore reduces rear recombination[14]. The concept of using P3HT to reduce recombination rates is recently demonstrated in a PbS solar cell[15]. Furthermore, the conductivity of P3HT can be modified[16,17] which is very useful for optimizing carrier extraction, fill factor and hence power conversion efficiency. By optimizing the extent of oxidation and the resultant thickness of P3HT layer, devices with P3HT performed, on average, 7.0 ± 0.4 % efficient, more than twice the average performance of devices without P3HT.

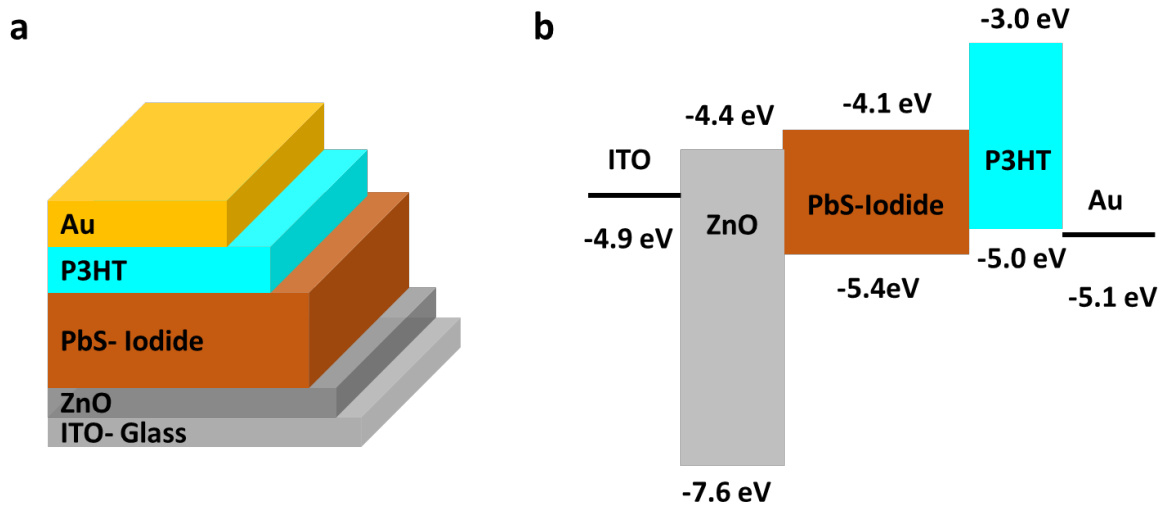

Figure 1. Device structure and band diagram. **a.** The device consists of about 100nm ZnO, 220nm PbS-Iodide, 100nm P3HT and 100nm Au. **b.** HUMO and LUMO levels of the various components and their values are cited from references [3,18]

EXPERIMENTAL SECTION

Synthesis of ZnO nanocrystals. ZnO nanocrystals were synthesized by using the method adapted from Pacholski *et al*[19]. 2.95 g of zinc acetate dihydrate was dissolved in 125 ml of methanol and kept, under stirring, at 60 ºC. 1.48 g of potassium hydroxide was dissolved in 65 ml of methanol. Then, potassium hydroxide solution was added dropwise to the zinc acetate solution and the reaction mixture was kept, under stirring, at 60 ºC for 2.5 h. ZnO nanocrystals were extracted by centrifugation at 6000 rpm and then washed twice by methanol followed by centrifugation. Finally, a mixture of 5 ml of chloroform and 5 ml of methanol was added to dissolve the precipitates and the solution was finally filtered with a 0.45 μm filter.

Synthesis of PbS CQDs. 1.3 eV PbS CQDs were synthesized using a method adapted from the literature[20]. 0.46 g of lead (II) oxide, 2 g of oleic acid (OA) and 10 g of octadecene (ODE) were mixed under vacuum at 90 °C for at least 2 hours, yielding a clear lead-oleate solution. The reaction temperature was further raised to 105 ºC and purged with N_2 gas. 210 µL of hexamethyldisilathiane was carefully mixed with 5 g of ODE and then rapidly injected into the lead-oleate solution. CQDs were purified by adding acetone, followed by centrifugation. The extracted CQDs were re-dispersed in hexane and were further precipitated twice with methanol, and then finally re-dispersed in octane 50 mg ml $^{-1}$.

Solution phase ligand exchange. PbS CQDs were diluted to a concentration of 10 mg/mL and 4 mL of this solution was added to 3 mL of methylammonium iodide in dimethylformamide (DMF) solution with a concentration of 80 mg/mL. The immiscible phases were vortexed vigorously and PbS CQDs were transferred into the DMF phase. The DMF phase was carefully

separated and toluene is added to precipitate the CQDs. The precipitates were finally dispersed in butylamine at 200 mg/mL concentration for film fabrication.

Device fabrication. Patterned ITO substrates (Delta Technologies Inc.) were cleaned thoroughly and then treated with O_2 plasma. A 100 ± 7 nm ZnO layer was deposited by spin-coating the prepared ZnO nanocrystal colloidal solution onto ITO at 2000 rpm for 30 s. A PbS-Iodide film was then deposited on the ZnO film by spin-coating 10 μL of exchanged PbS solution at 3000 rpm for 30 s and then annealed at 100ºC for 5 mins, which gave a film thickness of about 220 ± 7 nm. For devices with hole transporter, a 10 mg/mL P3HT in chlorobenzene solution was spin-coated above the PbS-Iodide layer at 1000 rpm for 45 s to form a 100 ± 5 nm film. For O_2 plasma treatment, the P3HT coated film was exposed to O_2 partial pressure of 120 mTorr for the required amount of time. Finally, the top electrodes were formed by depositing gold, using an Edwards 306 thermal evaporator system at 10^{-6} Torr, up to a thickness of 100 nm with an evaporation rate of 0.1 nm/s. A shadow mask was used to pattern the electrodes.

Material characterization. Work function data were taken by The KP Technology Scanning Kelvin Probe System 2001. For each sample, 25 data were measured for each of 3 arbitrarily chosen scanning points (75 data in total). At the beginning and the end of analysis, measurements of reference samples (Al: work function of 4.1 eV, and Au: work function of 5.1 eV) were used to generate a calibration curve. This calibration curve converts raw data, which are relative work function values with respect to the work function of the scanning probe, to absolute work function data. Fourier Transform Infrared (FTIR) spectroscopic measurement was carried out using Varian 660 Spectrometer in ATR mode. Samples were prepared by simply drop-casting P3HT in chlorobenzene solution on glass substrates. A NanoSIMS50 (CAMECA, France) was used to obtain compositional depth profiles of devices made without the top gold

contact. The Cs^+ source in the NanoSIMS was used, and $^{12}C^-$ $^{16}O^-$, $^{32}S^-$, $^{64}Zn^{16}O^-$ and $^{127}I^-$ signals were detected to measure the O/S count ratio and to identify layers in the solar cell. A probe current of ~6.9 pA was used for depth profiling. The NanoSIMS was set up to sputter an area of 20 μm by 20 μm, and signals from the central 10 μm by 10 μm area were counted to avoid artifacts from crater edges.

Device characterization. All devices were loaded into a sealed testing chamber flushed with N_2 to minimize sample degradation during testing. Current-voltage measurement was performed using a Keithley 2400 Source Meter. The voltage was swept from -0.5 V to 1.0 V and then in the reverse, at a step size of 0.025 V and a scan speed of 20 mV/s. Samples do exhibit some hysteresis. All performance metric cited in this manuscript is taken from the backward scan but hysteresis and full device metric are reported separately in the Supporting Information. AM1.5 solar spectrum illumination was simulated by a Newport solar simulator fitted with an AM1.5 filter. The power density of the light source was calibrated with an ABET technologies Si reference cell model 15151-KG5. External quantum efficiency was measured by illuminating the devices by a chopped monochromatic focused light source produced from a halogen lamp fitted with an Oriel Cornerstone 130 monochromator. White light bias was applied with a Thorlabs MWWHL3 white LED. Light intensity at different wavelengths was calibrated using a Newport 818 UV enhanced silicon photodetector and a Newport 918 IR germanium photodetector. The current signal was measured with a Keithley 6845 picoammeter and a lock-in amplifier. To measure photovoltage decay, a Thorlabs MWWHL3 white LED fitted with a DC2100 LED driver with PWM mode was used. Intensity was adjusted to reach device open circuit voltage, and light pulses were adjusted to 100 Hz with 30% duty cycle. The photovoltage

decay was captured on a Teledyne LeCroy WAVEJET 354 oscilloscope across the high impedance (1 M Ω) port.

RESULTS AND DISCUSSION

Our main device is comprised of a patterned ITO substrate spin coated with ZnO, PbS and P3HT layers and a vacuum thermally deposited top gold electrode, while the control device was made with the same thickness of PbS, without the P3HT layer. Before deposition, the 1.3 eV PbS CQDs in octane with oleic acid as their native ligand are first subjected to a solution phase ligand exchange procedure to yield iodide-capped PbS (henceforth termed PbS-Iodide), which is finally dissolved in butylamine to a concentration of approximately 200 mg/ml according to the procedure as described by Ning *et al*.[21] (See fig. S1). The fabrication process simply consists of only 3 spin coat steps in air ambient and a final thermal evaporation step.

A comparison of representative devices with and without P3HT is shown in fig. 2a. Devices with P3HT generally displayed improved short-circuit current (J_{sc}) and open-circuit voltage (V_{oc}) over the control devices. However, the as-fabricated P3HT devices exhibited a "roll-over effect" in the power quadrant of the *J-V* curve, limiting *FF* and overall *PCE*. This effect has been well documented by a number of authors to suggest the existence of a barrier to charge injection[8,22,23] If the devices were left in the dark and in air-ambient for 2 days, the roll-over effect was found to be eliminated and there was a marked improvement in fill factor and overall device performance (fig. 2b). We hypothesize that this improvement upon ageing is due to P3HT oxidation, which has been previously shown to cause *p*-type doping, shifting its HOMO-LUMO levels and increasing its work function[24]. To explore this further, Kelvin probe measurements were used to measure the Fermi energy (E_F) or work function position of PbS-Iodide and P3HT as prepared in an inert glove box atmosphere and after exposure to air. After two days, the change in the PbS-

Iodide E_F was negligible and it remained at -4.91 (±0.02) eV while the P3HT E_F dropped from -4.75 (±0.02) eV to -4.80 (±0.02) eV, bringing it closer to the PbS value and making hole injection more favorable at the interface (see fig. 2c, d). This is consistent with a systematic energy shifts of core-levels and HOMO levels on the oxidation of P3HT as observed by Hintz *et al.*[24].

The origin of improved device performance will be investigated based on the hypothesis that P3HT is acting as a combination of: i) an electron blocking layer minimizing rear contact recombination[12]; ii) a hole transport layer inhibiting the formation of space charge at the electrodes[7]; iii) a smoothing layer preventing shunt pathways; and iv) an optical spacer layer increasing reabsorption of light that is reflected off the rear electrode[25].

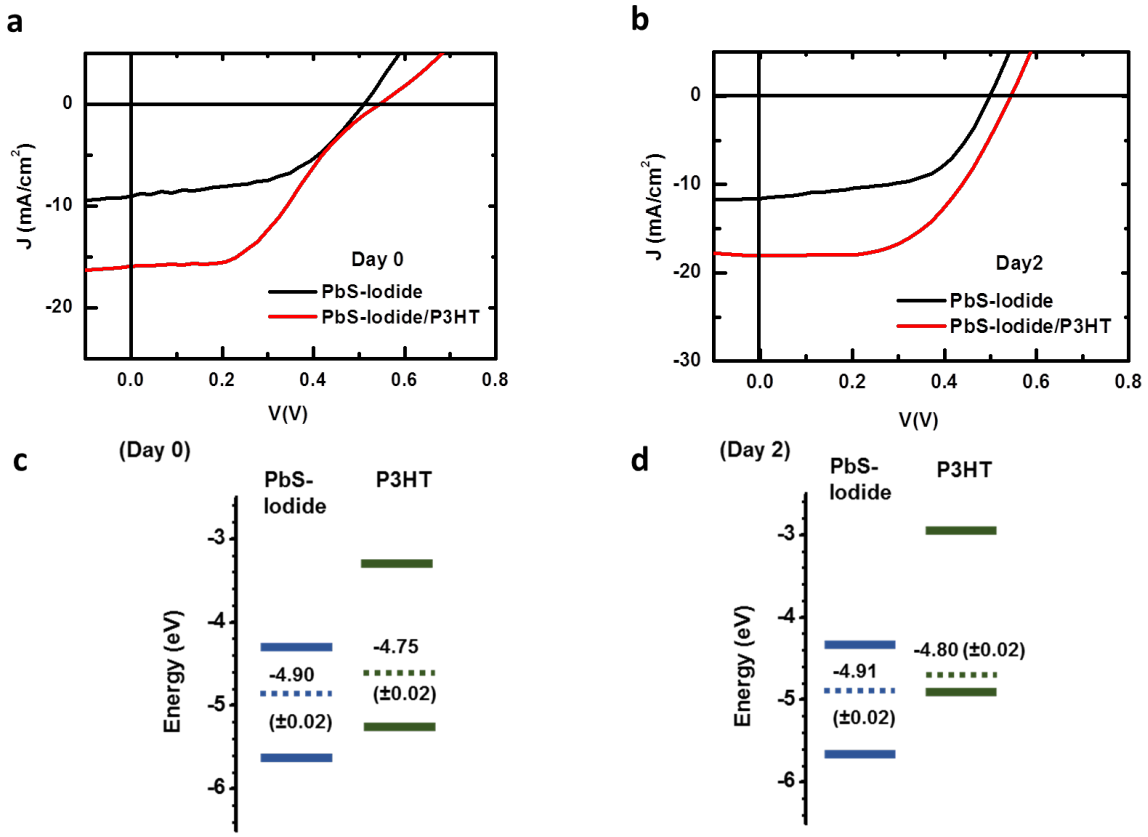

Figure 2. P3HT as a hole transporter and the effect of air storage. Device performance comparison, with and without the untreated P3HT hole transport layer, **a.** as fabricated and **b.** after 2 days of storage in air. **c.** Energy level diagram and position of Fermi level of the PbS active layer and P3HT as measured by scanning Kelvin probe on the day of fabrication and **d.** after 2 days of storage in air. The associated uncertainties are quoted in parenthesis.

To control the extent of oxidation, an O_2 plasma treatment was employed to physicochemically etch the P3HT. Various plasma exposure times were used, and fig. 3a shows how the *J-V* characteristics change as a function of etch time. A three second etch gave optimal device performance (J_{sc} 16.9 mA/cm^{-2}, V_{oc} 0.51 V, *FF* 0.63 and *PCE* 5.4 %). Kelvin probe measurements (fig. 3b) go in some way to explain this observation, as a three second etch results in a more negative E_F value of -5.04 ± 0.01 eV, which might encourage hole injection from the PbS-Iodide layer. *J-V* characterization showed no rollover effect on devices tested immediately after fabrication (see fig. 3c), which is not the case for devices without the P3HT O_2 plasma treatment (fig. 2a, b). The plasma treatment also thinned down the P3HT layer as shown in fig. S2b, and for the three second treatment, the P3HT thickness was reduced from 102 nm to 67.5nm. This most likely plays a secondary role in optimizing charge transport and collection in the device. Also, the 3 sec plasma treatment was determined to be short enough to effect the work function of the P3HT layer and not influencing the PbS-Iodide layer underneath (see fig. S4). Even though the work function of P3HT continued to increase with increasing treatment time, the device performance decreased. Over-treating the P3HT layer might result severe chemical degradation or over-doping, and the increased treatment length may result in the oxidation of the underlying PbS-Iodide layer. To investigate the effect of P3HT thickness on

device performance, devices with the same PbS-Iodide thickness but with different P3HT thicknesses were tested after 2 days of exposure to air and the performance results are shown in fig. 3d, e. V_{oc}, J_{sc} and *FF* all decreased with thinner P3HT layers, while too thick a P3HT layer gave high J_{sc} but with a lower *FF*. These trends follow very closely the work of Tress *et al*.[13], who showed that a sufficiently thick (~400 nm) layer of Spiro-MeOTAD was required to form an interface between the perovskite layer and top electrode. The reason for that thickness was mainly due to the relatively rough perovskite surface, so as to ensure that the hole transport material formed a smooth and uniform contact with the top electrode, thus reducing shunt pathways. However, it was also showed that beyond the optimal thickness, a thicker hole transport layer reduces *FF* due to greater series resistance. In our case, PbS-Iodide displayed a much smoother surface than the perovskites due to the solution phase ligand exchange method. Therefore, the other effect of plasma treatment is to thin down the P3HT layer slightly so as to reduce series resistance. We established that the optimum P3HT thickness for device *PCE* before the plasma treatment was about 100nm as shown in fig. 3e.

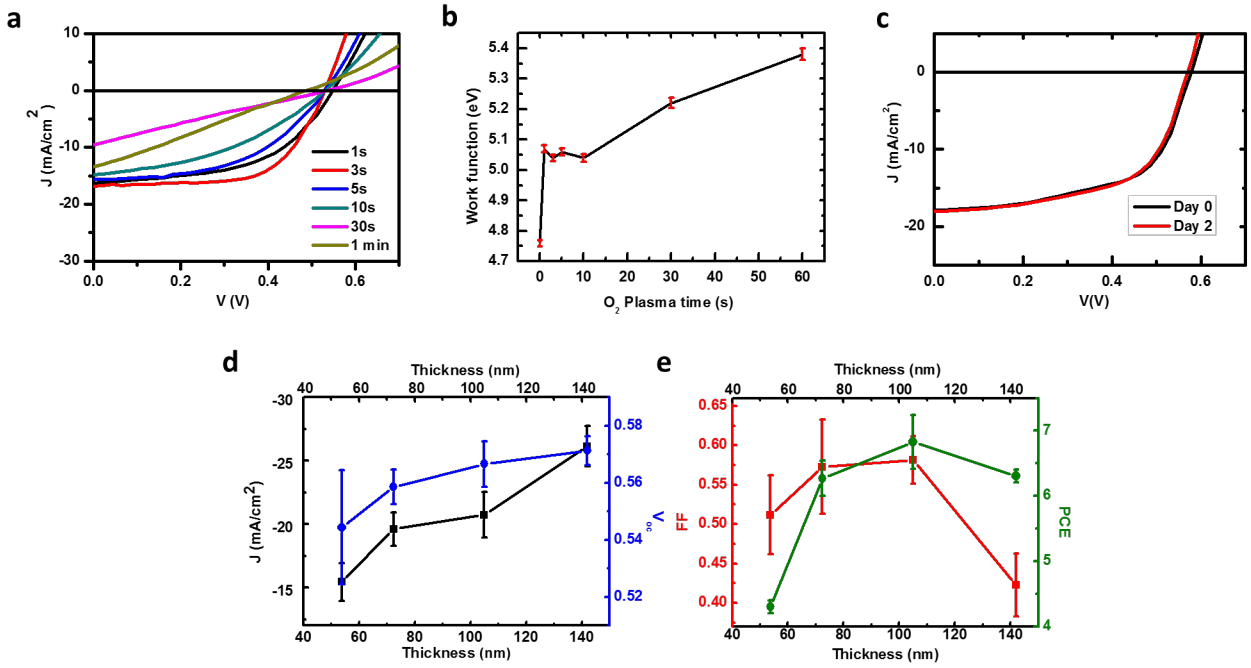

Figure 3. Effect of O_2 plasma treatment and the optimization of PbS-Iodide/P3HT devices. **a.** Device performances with P3HT layer exposed to increasing O_2 plasma treatment times. 3s is found to be the optimal treatment time for *PCE*. **b.** Scanning Kelvin probe measurements on P3HT with increasing O_2 plasma treatment times. **c.** Device performance, with P3HT layer exposed to 3s O_2 plasma treatment, when as-fabricated and then tested again after two days of air-ambient storage in the dark. **d.** Device J_{sc} and V_{oc}, **e.** *FF* and *PCE* with different thicknesses of P3HT layer. Results are obtained two days after fabrication to avoid the injection barrier effect.

To understand the chemical effect of the O_2 plasma treatment, UV-Vis-NIR absorption, Fourier Transform Infrared Spectroscopy (FTIR) and Secondary Ion Mass Spectrometry (SIMS) have been employed. The UV-Vis-NIR spectrum in fig. 4a shows how the absorption changed in the

P3HT with various O_2 plasma treatment times. The magnitude of absorbance is reduced, which is consistent with layer thinning and could also be ascribed to chemical degradation of the P3HT thiol ring due to oxidation. Oxidative degradation is also known to result in a blueshift in the absorption spectrum due to the reduction in molecular weight of the polymer chain[26]. However, in our case, the blueshift is minimal, which means that any oxidative effect of plasma mainly changes the chemical moiety in the polymer rather than cleaving it into to smaller fragments. This would be consistent with a *p*-type doping effect and Fermi level shift of P3HT[24]. Further, FTIR measurements (fig. 4b, c) showed evidence of increased oxidation of P3HT with 3 s O_2 plasma treatment: The O-H bonds at 3360cm^{-1} and C=O bonds at 1718cm^{-1} appeared upon plasma treatment while a slight degradation of the hydrocarbon peaks at 2800-2900cm^{-1} was recorded (fig. S5)[19,24].

SIMS was used to investigate the extent of oxidation by comparing the ratio of oxygen to sulfur counts between pristine, air-aged, and O_2 plasma treated P3HT-devices under the same experimental conditions (fig. 4d). The oxygen-sulfur ratio is measured and calculated to be higher in the air-aged sample and even greater in the O_2 plasma-treated sample. More oxygen was present throughout the thickness of P3HT layer in the plasma treated sample as compared to the air-aged sample. From this, we concluded that the extent of oxidation with plasma treatment was significantly greater than from air ageing alone. This increased oxygen to sulfur ratio had been similarly reported using X-ray photoelectron spectroscopy (XPS) with oxidized P3HT[24]. Therefore, we confirmed our hypothesis that the oxidation of the P3HT increased the work function [24], reduced the charge injection barrier and therefore “healed” the device performance.

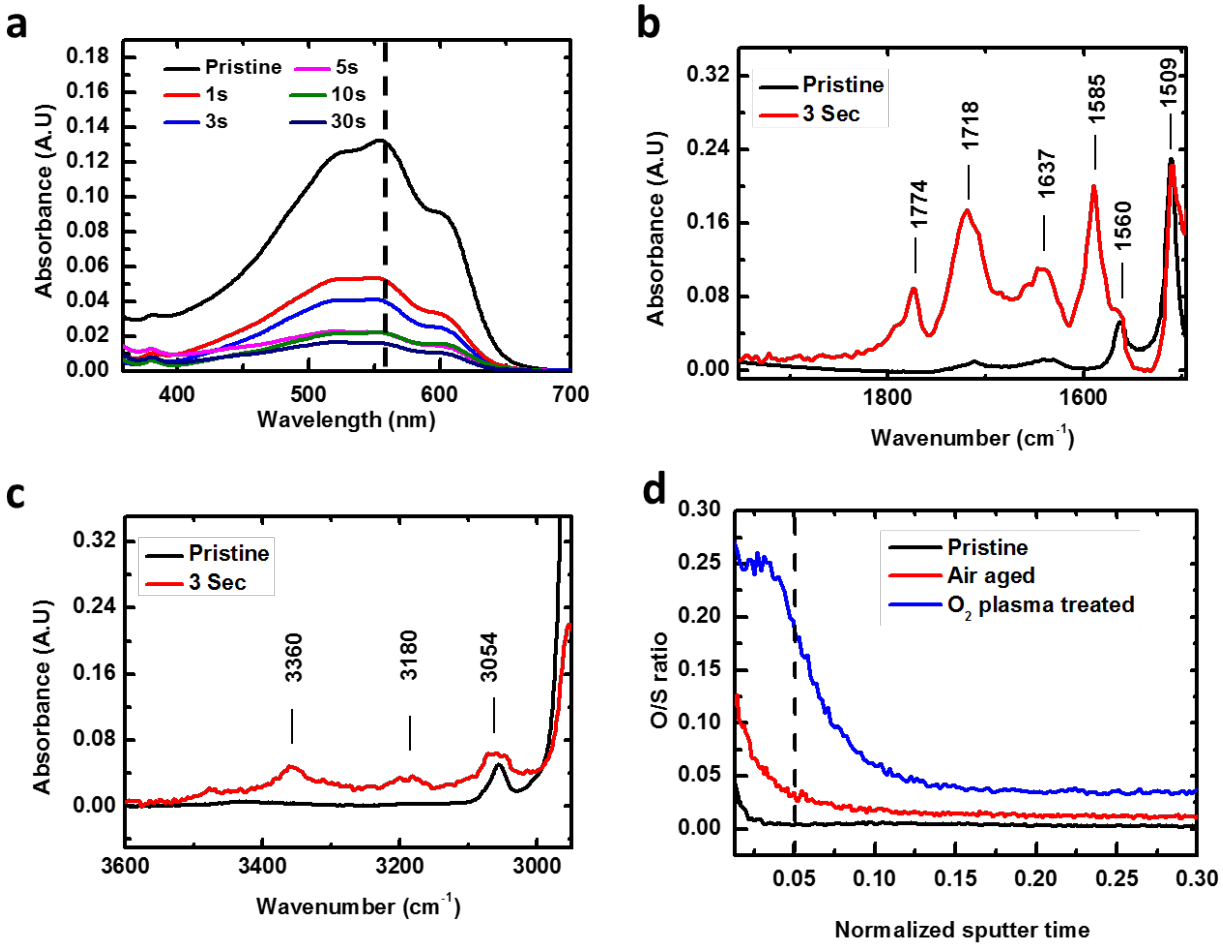

Figure 4. Material and compositional analysis of P3HT (pristine, air aged and O_2 plasma treated). **a.** UV-Vis absorbance spectra of P3HT films cast on glass slides which have been exposed to various O_2 plasma treatment times. **b.** FTIR spectrum showing the range of wavenumbers attributed to C=O stretching (1774 cm^{-1}, 1718 cm^{-1}, 1637 cm^{-1}, 1585 cm^{-1}) while 1560 cm^{-1} and 1509 cm^{-1} are associated with aromatic components in P3HT, and **c.** O-H stretching (3360 cm^{-1} and 3180 cm^{-1}) while 3054 cm^{-1} is associated with aromatic C-H bonds[27]. **d.** Ratio of oxygen to sulfur counts as determined by SIMS, dotted line shows the approximate position of the end of P3HT component and the start of PbS-Iodide, which is determined from depth profile analysis (refer to fig. S6 for more details).

To show the importance of using a hole transport layer to improve the balance of charge collection, the optoelectronic properties of test devices with and without the P3HT layer, and with O_2 plasma treated P3HT (hereby termed P3HT:O_2) were investigated. Fig. 5a depicts light intensity dependence J_{sc} traces of devices with and without the P3HT layer, and the measurements of all these devices were taken at day 2 of storage in air- ambient and dark. Results were fitted to a power law relation, $J = bI^a$, where J refers to current density, I is the light intensity and a, b are arbitrary constants. When a=1, device operation is ideal and charge extraction balanced with minimal bimolecular recombination. a <1 indicates a deviation from balanced charge transport resulting in the formation of space charge[28]. Devices with the hole transporter layer have a values approaching the value of 1, which is consistent with the high fill factors observed. On the other hand, the lack of hole transport layer would possibly result in a space charge-limited current extraction, which resulted in greater bimolecular recombination[29]. Open-circuit voltage decay measurements were also performed as shown in fig. 5b. Under open-circuit conditions, charges build up under illumination and longer charge lifetimes signify a pronounced reduction in carrier recombination[30] as seen in the case when P3HT was used.

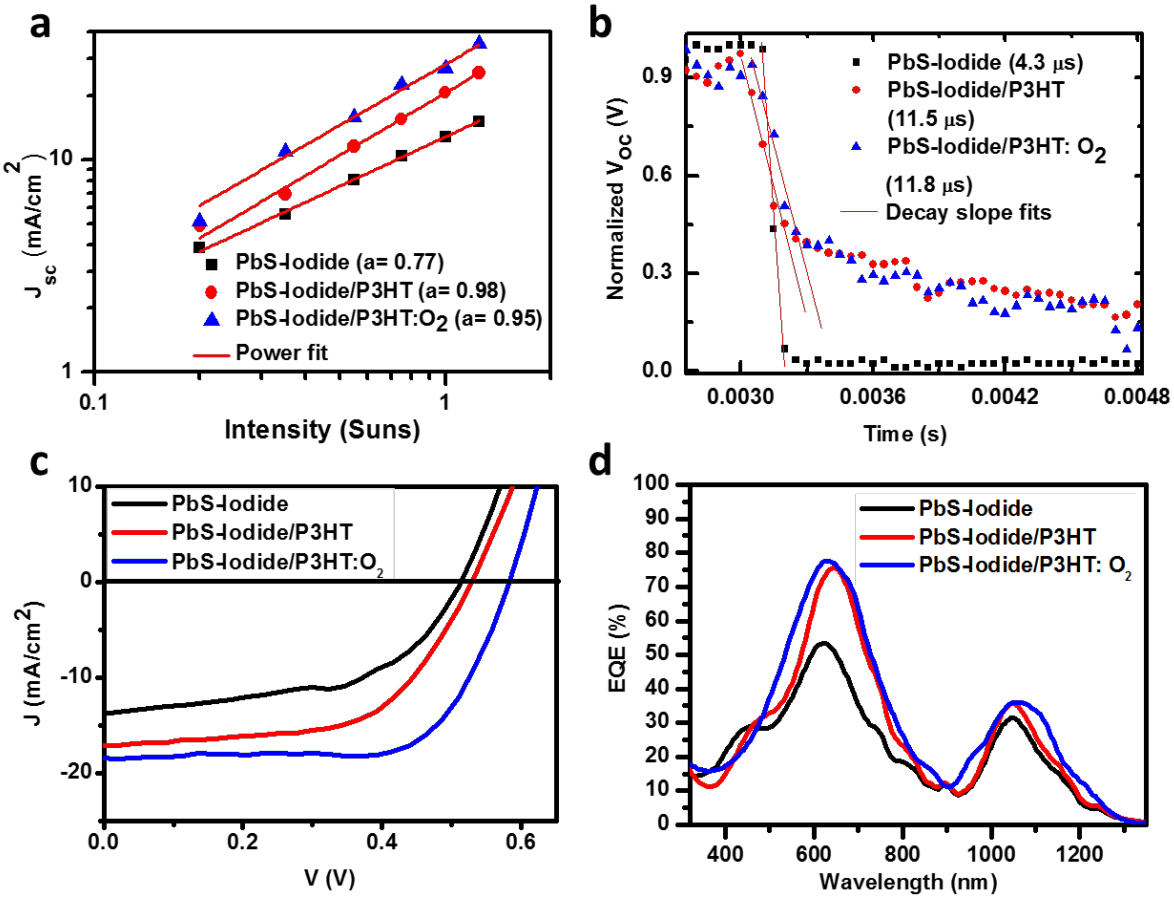

Figure 5. Champion photovoltaic devices and their performance. **a.** Intensity dependent short-circuit current trace of the devices with and without P3HT and O_2 treated P3HT, with the proposed power law fit. Fitted power exponent with standard errors are: a_1=0.77 (± 0.02) for PbS-Iodide, a_2=0.98 ± 0.05 for PbS-Iodide/P3HT and a_3=0.95 ± 0.07 for PbS-Iodide/P3HT:O_2. **b.** Open-circuit voltage decay of the same devices with lifetime quoted in parentheses. **c.** *J-V* sweeps showing photovoltaic performance under AM1.5 illumination of device with 100 nm of P3HT, without P3HT and with O_2 treated P3HT. Measurements were taken two weeks after fabrication, where device performance has stabilized. Please refer to fig. S7 for hysteresis analysis. **d.** External quantum efficiencies of the corresponding devices.

n-type ZnO thin films are known to possess high carrier density[31] and are commonly used as electron selective contacts. Without P3HT, the device lacked symmetry and with electron collection dominating, this possibly led to space charge accumulation that would impede efficient charge transport[7]. Suitably doped P3HT has a Fermi energy level that allows a more ideal band alignment to extract holes from PbS layers and with a relatively high LUMO position, P3HT effectively blocks electrons at the rear electrode, thus reducing recombination. Therefore, having both electron and hole selective contacts would aid charge extraction in the diffusive transport regime[7]. Thus, at high forward bias, where the internal field is weaker and the depletion width is small, diffusive transport takes precedence and with charge selective contacts, a higher photocurrent could be sustained, leading to higher fill factors. Another interpretation of these results is that P3HT served as a buffer layer that would reduce Fermi level pinning effects, which are known to exist between gold and PbS[8]. These factors led to improved charge extraction as compared to device without P3HT, leading to better J_{sc}, V_{oc} and *FF* values as evident in fig. 5c. Furthermore, the significant improvement of the J_{sc} of P3HT devices could mostly be attributed to second pass absorption due to the presence of P3HT acting as a spacer layer, as decribed by Tress *et al*[25]. However, it must be noted that the devices do exhibit some hysteresis and results could be found in the Supporting Information (fig. S7 and table ST1).

Devices with fill factors as high as 0.70 were fabricated (refer to table 1 for device performance summary) and there is a marked device improvement as compared with devices without the P3HT layer. We believe that using an O_2 plasma treatment simultaneously controls both the extent of P3HT oxidation and film thickness. The external quantum efficiency measurement in fig. 5d showed a higher photocurrent extracted across the whole wavelength range, in particular near 600nm where photogenerated charges are produced mainly in the middle of the device. The

improvement of charge extraction in the middle regions of the device supports the hypothesis that an improvement in carrier lifetimes and the reduced charge recombination in devices with P3HT are due to the charge selectivity of P3HT and the elimination of space-charge limited transport.

In addition, the fabricated devices were stable in air: device performance metrics as a function of time are shown in fig. 6. P3HT is susceptible to oxidation and this oxidation causes *p*-type doping and shifts the Fermi energy level, resulting in favorable band alignment and hole injection. Therefore, when P3HT is fully oxidized, the device performance stabilizes and this can be seen in our O_2 plasma treated P3HT devices where the performance is stable on storage. Studies have shown that devices which utilized hole transport layers like MoO_3 worked well as fabricated, but the changes in work function over time degraded device performances[2].

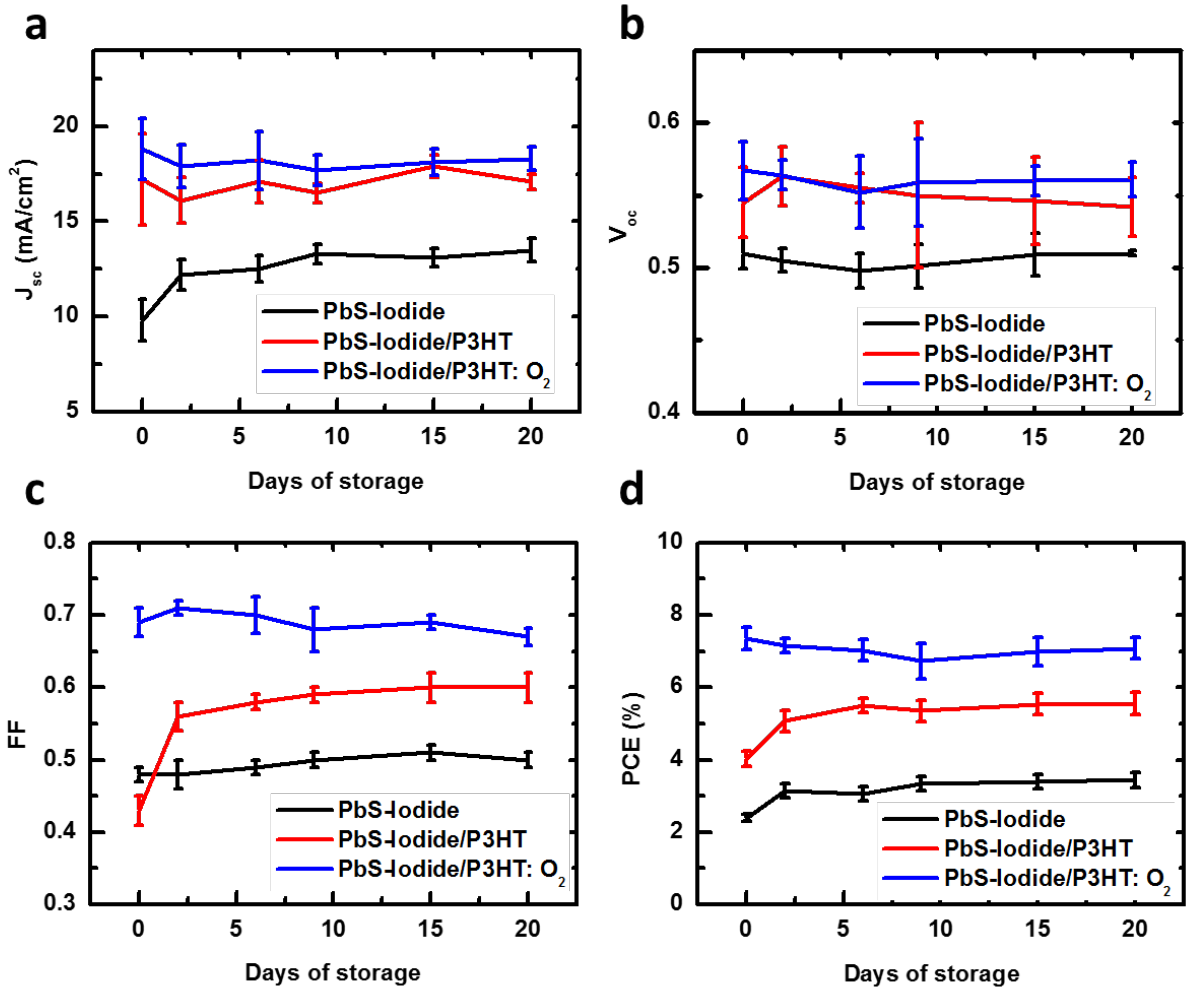

Figure 6. The variation of photovoltaic performance metrics of devices, with and without P3HT and O_2 treated P3HT, with storage time. **a.** short-circuit current, **b.** open-circuit voltage, **c.** fill factor and **d.** power conversion efficiency. The devices were unencapsulated and were stored in air between each measurements in a dark environment without any humidity control. The standard deviation (error bars) and the average (data point) were calculated from a sample of 9 devices on 3 separate substrates.

Table 1. Photovoltaic device performance summary.

Structure	J_{sc} (mA/cm^2)	V_{oc} (V)	*FF*	*PCE* (%)

ZnO/PbS-Iodide/Au	12.6± 2.3 (13.8)	0.51± 0.06 (0.51)	0.49± 0.05 (0.56)	3.1±0.4 (3.9)
ZnO/PbS-Iodide/P3HT/Au	16.2± 1.5 (17.1)	0.53± 0.03 (0.53)	0.61± 0.04 (0.59)	5.2±0.3 (5.3)
ZnO/PbS-Iodide/P3HT:O_2 treated 3s/Au	17.6± 1.7 (18.4)	0.56± 0.02 (0.58)	0.65± 0.03 (0.70)	6.4±0.4 (7.5)
The measurements for the best-performing cells are quoted in parenthesis. The reported averages and standard deviations are derived from 9 devices on 3 separate substrates from measurements performed after 2 weeks of air exposure (and storage in the dark). Results shown here are taken from the backward scans at a rate of 20 mV/s.				

CONCLUSION

In conclusion, we have shown that P3HT is a suitable hole transport layer in between the PbS CQD and the gold contact. P3HT performed the roles of regulating charge transport, reducing charge recombination, aiding to interface between the rougher PbS CQD film and gold electrode, as well as to act as a spacer layer for second pass absorption. We found that by oxidizing P3HT, its Fermi energy level was lowered, resulting in improved band alignment and sustained hole injection from the PbS layer even at high forward biases. In addition, devices were air stable over extended periods and in fact, mild oxidation is shown to be beneficial. An investigation of controlled oxidation indicates that *p*-doped P3HT served as an excellent hole transport material and also a charge selective contact. This was shown to reduce recombination, balance hole and electron extraction, and thereby reducing space charge effects. All these factors, together with second pass absorption effect contributed to higher J_{sc} and *FF* values when compared to devices without a P3HT layer. Optimized oxidation conditions and P3HT thickness were used to maximize device performance. The open-circuit voltages of our devices are still limited to below 0.6 V and they have to be improved to attain higher device efficiency. We believe that the

controlled modification of surface chemistry and removing sub-band gap states are key to V_{oc} improvements.

ASSOCIATED CONTENTS

Supporting information

More UV-Vis, wide scan FTIR data, scanning Kelvin probe on work function data and SIMS depth profile data are provided in a separate supporting information document. This material is available free of charge via the Internet at http://pubs.acs.org.

AUTHOR INFORMATION

Corresponding Author

* Professor Andrew A. R. Watt

email: andrew.watt@materials.ox.ac.uk

Tel: +44 1865 613455 or +44 7828 598301. Fax: +44 1865 273789

Author Contributions

The manuscript was written through contributions of all authors. All authors have given approval to the final version of the manuscript. ‡These authors contributed equally.

Funding Sources

We acknowledge funding from EPSRC (Platform Grant EP/ F048009/1).

Notes

The authors declare no competing financial interest.

ACKNOWLEDGMENT

D.C.J.N. acknowledges A*STAR for sponsoring the overseas research scholarship – NSS-PhD

REFERENCES

(1) NREL. Best Research-Cell Efficiency Chart. NREL 2016.
(2) Chuang, C.-H. M.; Brown, P. R.; Bulović, V.; Bawendi, M. G. Improved Performance and Stability in Quantum Dot Solar Cells through Band Alignment Engineering. *Nat. Mater.* **2014**, *13*, 796–801.
(3) Ning, Z.; Voznyy, O.; Pan, J.; Hoogland, S.; Adinolfi, V.; Xu, J.; Li, M.; Kirmani, A. R.; Sun, J.-P.; Minor, J.; Kemp, K. W.; Dong, H.; Rollny, L.; Labelle, A.; Carey, G.; Sutherland, B.; Hill, I.; Amassian, A.; Liu, H.; Tang, J.; Bakr, O. M.; Sargent, E. H. Air-Stable N-Type Colloidal Quantum Dot Solids. *Nat. Mater.* **2014**, *13* (8), 822–828.
(4) Zhitomirsky, D.; Voznyy, O.; Levina, L.; Hoogland, S.; Kemp, K. W.; Ip, A. H.; Thon, S. M.; Sargent, E. H. Engineering Colloidal Quantum Dot Solids within and beyond the Mobility-Invariant Regime. *Nat. Commun.* **2014**, *5*, 3803.
(5) Kramer, I. J.; Minor, J. C.; Moreno-Bautista, G.; Rollny, L.; Kanjanaboos, P.; Kopilovic, D.; Thon, S. M.; Carey, G. H.; Chou, K. W.; Zhitomirsky, D.; Amassian, A.; Sargent, E. H. Efficient Spray-Coated Colloidal Quantum Dot Solar Cells. *Adv. Mater.* **2015**, *27* (1), 116–121.
(6) Labelle, A. J.; Thon, S. M.; Masala, S.; Adachi, M. M.; Dong, H.; Farahani, M.; Ip, A. H.; Fratalocchi, A.; Sargent, E. H. Colloidal Quantum Dot Solar Cells Exploiting Hierarchical Structuring. *Nano Lett.* **2015**, *15* (2), 1101–1108.
(7) Mora-Sero, I.; Bertoluzzi, L.; Gonzalez-Pedro, V.; Gimenez, S.; Fabregat-Santiago, F.; Kemp, K. W.; Sargent, E. H.; Bisquert, J. Selective Contacts Drive Charge Extraction in Quantum Dot Solids via Asymmetry in Carrier Transfer Kinetics. *Nat. Commun.* **2013**, *4*, 2272.
(8) Gao, J.; Luther, J. M.; Semonin, O. E.; Ellingson, R. J.; Nozik, A. J.; Beard, M. C. Quantum Dot Size Dependent $J-V$ Characteristics in Heterojunction ZnO/PbS Quantum Dot Solar Cells. *Nano Lett.* **2011**, *11* (3), 1002–1008.
(9) Crisp, R. W.; Kroupa, D. M.; Marshall, A. R.; Miller, E. M.; Zhang, J.; Beard, M. C.; Luther, J. M. Metal Halide Solid-State Surface Treatment for High Efficiency PbS and PbSe QD Solar Cells. *Sci. Rep.* **2015**, *5*, 9945.
(10) Snaith, H. J. Perovskites: The Emergence of a New Era for Low-Cost, High-Efficiency Solar Cells. *J. Phys. Chem. Lett.* **2013**, *4* (21), 3623–3630.
(11) Lattante, S. Electron and Hole Transport Layers: Their Use in Inverted Bulk Heterojunction Polymer Solar Cells. *Electronics* **2014**, *3* (1), 132–164.
(12) Bi, D.; Yang, L.; Boschloo, G.; Hagfeldt, A.; Johansson, E. M. J. Effect of Different Hole Transport Materials on Recombination in $CH_3NH_3PbI_3$ Perovskite-Sensitized Mesoscopic Solar Cells. *J. Phys. Chem. Lett.* **2013**, *4* (9), 1532–1536.

(13) Marinova, N.; Tress, W.; Humphry-Baker, R.; Dar, M. I.; Bojinov, V.; Zakeeruddin, S. M.; Nazeeruddin, M. K.; Grätzel, M. Light Harvesting and Charge Recombination in $CH_3NH_3PbI_3$ Perovskite Solar Cells Studied by Hole Transport Layer Thickness Variation. *ACS Nano* **2015**, *9* (4), 4200–4209.
(14) Ludwigs, S.; Andrienko, D.; SpringerLink (Online service). *P3HT Revisited: From Molecular Scale to Solar Cell Devices*; 2014.
(15) Zhang, X.; Justo, Y.; Maes, J.; Walravens, W.; Zhang, J.; Liu, J.; Hens, Z.; Johansson, E. M. J. Slow Recombination in Quantum Dot Solid Solar Cell Using P–i–n Architecture with Organic P-Type Hole Transport Material. *J Mater Chem A* **2015**, *3* (41), 20579–20585.
(16) Park, S. K.; Kim, Y. H.; Han, J. I.; Moon, D. G.; Kim, W. K.; Kwak, M. G. Electrical Characteristics of Poly (3-Hexylthiophene) Thin Film Transistors Printed and Spin-Coated on Plastic Substrates. *Synth. Met.* **2003**, *139* (2), 377–384.
(17) Ukai, S.; Ito, H.; Marumoto, K.; Kuroda, S. Electrical Conduction of Regioregular and Regiorandom Poly(3-Hexylthiophene) Doped with Iodine. *J. Phys. Soc. Jpn.* **2005**, *74* (12), 3314–3319.
(18) Dou, L.; You, J.; Yang, J.; Chen, C.-C.; He, Y.; Murase, S.; Moriarty, T.; Emery, K.; Li, G.; Yang, Y. Tandem Polymer Solar Cells Featuring a Spectrally Matched Low-Bandgap Polymer. *Nat. Photonics* **2012**, *6* (3), 180–185.
(19) Pacholski, C.; Kornowski, A.; Weller, H. Self-Assembly of ZnO: From Nanodots to Nanorods. *Angew. Chem. Int. Ed Engl.* **2002**, *41* (7), 1188–1191.
(20) Hines, M. A.; Scholes, G. D. Colloidal PbS Nanocrystals with Size-Tunable Near-Infrared Emission: Observation of Post-Synthesis Self-Narrowing of the Particle Size Distribution. *Adv. Mater.* **2003**, *15* (21), 1844–1849.
(21) Ning, Z.; Dong, H.; Zhang, Q.; Voznyy, O.; Sargent, E. H. Solar Cells Based on Inks of N-Type Colloidal Quantum Dots. *ACS Nano* **2014**, *8* (10), 10321–10327.
(22) Demtsu, S. H.; Sites, J. R. Effect of Back-Contact Barrier on Thin-Film CdTe Solar Cells. *Thin Solid Films* **2006**, *510* (1-2), 320–324.
(23) Kouskoussa, B.; Morsli, M.; Benchouk, K.; Louarn, G.; Cattin, L.; Khelil, A.; Bernède, J. C. On the Improvement of the Anode/organic Material Interface in Organic Solar Cells by the Presence of an Ultra-Thin Gold Layer. *Phys. Status Solidi A* **2009**, *206* (2), 311–315.
(24) Hintz, H.; Peisert, H.; Egelhaaf, H.-J.; Chassé, T. Reversible and Irreversible Light-Induced P-Doping of P3HT by Oxygen Studied by Photoelectron Spectroscopy (XPS/UPS). *J. Phys. Chem. C* **2011**, *115* (27), 13373–13376.
(25) Tress, W.; Marinova, N.; Inganas, O.; Nazeeruddin, M. K.; Zakeeruddin, S. M.; Graetzel, M. The Role of the Hole-Transport Layer in Perovskite Solar Cells - Reducing Recombination and Increasing Absorption; IEEE, 2014; pp 1563–1566.
(26) Peters, V.; Tumkur, T. U.; Noginov, M. A. Control of Chemical Reactions in the Vicinity of Hyperbolic Metamaterials and Metallic Surfaces; OSA, 2014; p FM1C.6.
(27) Silverstein, R. M. *Spectrometric Identification of Organic Compounds*, Eighth edition.; John Wiley and Sons, Inc: Hoboken, NJ, 2015.
(28) Koster, L. J. A.; Mihailetchi, V. D.; Xie, H.; Blom, P. W. M. Origin of the Light Intensity Dependence of the Short-Circuit Current of Polymer/fullerene Solar Cells. *Appl. Phys. Lett.* **2005**, *87* (20), 203502.
(29) Mihailetchi, V.; Wildeman, J.; Blom, P. Space-Charge Limited Photocurrent. *Phys. Rev. Lett.* **2005**, *94* (12), 126602.

(30) Sharma, S. K.; Tewary, V. K. Theory of Open-Circuit Photovoltage Decay in a Finite Base Solar Cell with Drift Field. *J. Phys. Appl. Phys.* **1982**, *15* (6), 1077–1087.
(31) Lakhwani, G.; Roijmans, R. F. H.; Kronemeijer, A. J.; Gilot, J.; Janssen, R. A. J.; Meskers, S. C. J. Probing Charge Carrier Density in a Layer of Photodoped ZnO Nanoparticles by Spectroscopic Ellipsometry. *J. Phys. Chem. C* **2010**, *114* (35), 14804–14810.

Table of Contents Graphic